Eur. Phys. J. Plus (2023) 138:47
https://doi.org/10.1140/epjp/s13360-022-03632-4

THE EUROPEAN PHYSICAL JOURNAL PLUS

Regular Article

Simulated image of the shadow of the Kerr–Newman–NUT–Kiselev black hole in the Rastall gravity with a thin accretion disk

Temurbek Mirzaev[1,2,a], **Song Li**[3,4,b], **Bakhtiyor Narzilloev**[5,6,7,8,c], **Ibrar Hussain**[9,d], **Ahmadjon Abdujabbarov**[2,5,8,10,11,e], **Bobomurat Ahmedov**[2,4,8,f]

[1] Department of Physics, Center for Field Theory and Particle Physics, Fudan University, Shanghai 200438, China
[2] National University of Uzbekistan, Tashkent 100174, Uzbekistan
[3] Shanghai Astronomical Observatory, Shanghai 200030, China
[4] School of Astronomy and Space Science, University of Chinese Academy of Sciences, Beijing 100049, China
[5] Ulugh Beg Astronomical Institute, Astronomy St. 33, Tashkent 100052, Uzbekistan
[6] Akfa University, Milliy Bog' Street 264, Tashkent 111221, Uzbekistan
[7] Samarkand State University, University Avenue 15, Samarkand 140104, Uzbekistan
[8] Tashkent Institute of Irrigation and Agricultural Mechanization Engineers, Kori Niyoziy 39, Tashkent 100000, Uzbekistan
[9] School of Electrical Engineering and Computer Science, National University of Sciences and Technology, H-12, Islamabad, Pakistan
[10] Institute of Nuclear Physics, Ulugbek 1, Tashkent 100214, Uzbekistan
[11] Tashkent State Technical University, Tashkent 100095, Uzbekistan

Received: 1 August 2022 / Accepted: 26 December 2022

Abstract Here, we study the effect of strong gravitational field on the light rays emitted from the particles in the accretion disk in the vicinity of the Kerr–Newman–NUT–Kiselev (KNNK) black hole in the Rastall gravity (RG). In our analysis we consider the thin accretion disk model of Novikov and Thorne. We observe that the thermal flux of the accretion disk strongly depends on the intensity of the quintessence in the spacetime of the KNNK black hole in the RG, and the flux decreases for the increasing values of the quintessential intensity. We also notice that the smaller values of the equation of state parameter ω_q, for the quintessence, reduces the thermal flux for very small values of the Rastall parameter $\kappa\lambda$. Further we use the numerical codes, namely, the GYOTO and TM (Temurbek Mirzaev) codes, using C++ and Python languages, to compare the shadow cast by the KNNK black hole in the RG. We see that both the codes give similar behavior of the shadow cast by the KNNK black hole in the RG. Interestingly, we observe that the left hand side of the apparent black hole environment with respect to the central black hole is much brighter than the right hand side. This is due to the Doppler effect, i.e. the frequency of photons coming towards the observer (and thus the observed flux energy) is always higher than those of moving away form the observer. We demonstrate that increase of the quintessential intensity increases the size of the shadow cast by the KNNK black hole in the RG, considerably when the parameter $\kappa\lambda$ is very close to zero. We also see that the change in the size of the shadow of the KNNK black hole in the RG becomes negligible with the change in the quintessential intensity parameter α, when the parameter ω_q is close to zero and it becomes considerable when the parameter ω_q is smaller than zero. Next, we show that the position and shape of the shadow cast by the KNNK black hole in the RG strongly depends on the inclination angle of the incident light. We notice that the shadow of the KNNK black hole in the RG has more circular-like form for smaller values of the inclination angle. Further the shadow of the KNNK black hole in the RG shifts towards the right and becomes more deformed with the increasing values of the inclination angle.

1 Introduction

To acquire knowledge about the geometric structure of a spacetime and to understand the gravitational field of ultra-compact objects like black holes, the study of particle motion in black hole spacetimes is a useful tool for this purpose. Usually two types of geodesic motion in black hole spacetimes are considered, namely, timelike geodesic and null geodesics. The study of the latter one is important from the point of view as it can be related to the shadow cast by black holes. When a photon or light passes a nearby black hole,

[a] e-mail: mtemur141096@gmail.com
[b] e-mail: leesong@shao.ac.cn
[c] e-mail: nbakhtiyor18@fudan.edu.cn
[d] e-mail: ibrar.hussain@seecs.nust.edu.pk (corresponding author)
[e] e-mail: ahmadjon@astrin.uz
[f] e-mail: ahmedov@astrin.uz

Published online: 19 January 2023

according to the Einstein theory of General Relativity (GR), it gets deflected by the strong gravitational field of the central black hole and it may go in circular orbits. These circular orbits of photons are also called light rings. As a result of these light rings around a black hole, the central object i.e the black hole appears as a dark disk in the sky and in the literature it is known as the black hole shadow. Falcke et al. introduced the idea of observing the black hole shadow at the galactic centre SgrA* with very long baseline interferometry (VLBI) at the level of submillimeter wavelengths, where they assumed thin accretion flow in the region of the spectrum [1]. The recent observation of the shadow of the supermassive black hole at the centre of the galaxy M87, by the Event Horizon Telescope (EHT) Collaboration [2], has given a boost to the study of black hole shadows. The estimate of the masses of black hole has already been obtained and the black holes are now classified according to their masses as primordial black holes, stellar-mass black holes and supermassive black holes [3]. The other important parameter of a rotating black hole is its spin which may be related with the distortion of the shadow cast by the black hole. The estimation of the spin of a black hole is still an unresolved issue. Amongst different mechanisms proposed for the measurement of the spin of a black hole, the black hole shadow is a potential candidate to provide useful information about the estimation of the spin parameter of a rotating black hole [4].

The comprehension of the process of the formation of an accretion disk around a rotating black hole is an interesting topic of research [5]. Different models have been proposed to study the accretion disks around black holes [6, 7]. Using these models the accretion of different types of matter have been analysed in a variety of black hoe spacetimes [8–11]. The model of thin accretion disk was presented by Shakura and Sunyaev in the Newtonian gravity background [6]. The Shakura and Sunyaev model of the thin accretion disk was then extended by Novikov and Thorne in the framework of GR by considering the equatorial accretion on the Kerr black hole [12]. In the Novikov–Thorne model they assumed that the accretion rate of the matter on the black hole is constant and is independent of the radius of the disk. The energy flux of the accretion disk was then studied by Page and Thorne [7]. The accretion disk has also been analysed in the theories of gravity other than GR [13–18]. The study of accretion disk has also been carried out in other compact objects like wormhole and neutron stars [19–22]. Besides the analytical studies of the accretion disks around black holes, numerical studies have also been done in black hole geometries [23–26]. Different numerical codes have been developed to investigate the black hole shadow cast by black holes in the presence of the accretions disks [27, 28]. Vincent et al. have given a general relativistic ray-tracing code known as GYOTO code for the computation of the images of the astronomical compact objects in the surrounding of black holes and other ultra-compact objects in the sky [28]. The GYOTO code also provides the trajectories of massive objects in the relativistic regime as it can integrate the null and timelike geodesic equations in the spacetime metric of the compact objects. Recently another ray tracing code has been proposed by Temurbek, which is a modified version of the codes described in [29–31] and is applied in the current analysis.

From the recent observations, the existence of a repulsive gravitational force at the global scale (cosmic dark energy), which may be responsible for the current accelerated expansion of the observable Universe has been confirmed [32]. One of the candidates for the dark energy is the quintessential dark energy and is characterized by the equation of state $P_q = \omega_q \rho_q$, where P_q, ρ_q and ω_q are pressure, energy density and the parameter of the equation of state, respectively. The parameter ω_q is restricted as $-1 < \omega_q < -1/3$ for the quintessence. In an astrophysical situation the quintessential dark energy can give rise to some gravitational effects in the vicinity of black holes, as, for example, deflecting the photons or light coming from some distant star, and therefore, should be taken into account in this scenario. To know the role played by the quintessential dark energy in such a situation, Kiselev has obtained a black hole solution of the Einstein field equations of GR for a point gravitating source both with and without charge [33]. The Kislev solution was then generalized for an axially symmetric gravitating source [34], and the charged version of the same was then presented in the literature [33]. The charged-Kiselev black hoe has also been studied with the NUT parameter [35], which can be interpreted either as a parameter for the gravitomagnetic monopole of the central gravitational source or as a property responsible for the twisting of the surrounding spacetime [36]. The charged rotating Kiselev black hole in the presence of the NUT parameter has also been studied in the Rastall theory of gravity [37]. The Rastall theory of gravity is an alternative to the GR, where the matter field is non-minimally coupled to the geometry [38]. Visser objected the Rastall theory of gravity by arguing that it is equivalent to the GR [39]. Replying to the Visser claim, Darbari et al., presented that the Rastall theory is not equivalent to the GR and is an alternative theory of gravity which is to be consider as an open theory in comparison of the GR [40]. In the Rastall theory of gravity static as well as rotating black hole solutions have been obtained [41, 42]. In a recent work geodesic motion has been studied in the spacetime of the charged-rotating-NUT Kiselev black hole in the Rastall theory of gravity, where the imprints of the Rastall parameter have been analysed on the quasi periodic oscillations of particles in the stable circular orbits [43]. For interested readers, we recommend to see our previously published papers [44–50].

In the present study we are exploring the black hole shadow cast by the KNNK black hole in the RG, along with the thin accretion disk around it. For this purpose we are considering the Novikov–Thorne thin accretion disk model. Further we use the GYOTO code and the TM (Temurbek Mirzaev) code to compare the results obtained from both the codes for the images of the KNNK black hole. We observe that the thermal flux of the thin accretion disk of Novikov and Thorne is strongly dependent on the quintessential intensity and the Rastall parameter of the KNNK black hole spacetime in the RG. We see that the thermal flux becomes weaker for the bigger values of the quintessential intensity. Next, we use GYOTO code and TM code to explore the shadow formed around the KNNK black hole in the RG, with a thin accretion disk, and compare the results obtained using the two codes. The details are given in the subsequent sections.

This work is organized as follows: In the next section, the KNNK black hole in the Rastall theory of gravity is briefly reviewed. In Sect. 3 the Novikov–Thorne accretion disk model is discussed. In the Sect. 4 the shadow cast by the KNNK black hoe in the

Table 1 Exact analytical solutions for the inner and outer horizons of the KNNK black hole in the RG for selected values of parameters ω_q and $\kappa\lambda$

$\omega_q, \kappa\lambda$	Horizon ($r_\pm$)
0,0	$\left(M+\frac{\alpha}{2}\right) \pm \sqrt{\left(M+\frac{\alpha}{2}\right)^2 + l^2 - a^2 - q^2}$
− 1/3,0	$\frac{M}{1-\alpha} \pm \frac{\sqrt{M^2-(a^2+q^2-l^2)(1-\alpha)}}{1-\alpha}$
0,1/6	$\frac{M}{1-\alpha} \pm \frac{\sqrt{M^2-(a^2+q^2-l^2)(1-\alpha)}}{1-\alpha}$
− 1/3,− 1/2	$\left(M+\frac{\alpha}{2}\right) \pm \sqrt{\left(M+\frac{\alpha}{2}\right)^2 + l^2 - a^2 - q^2}$
1/3,0	$M \pm \sqrt{M^2 + l^2 + \alpha - a^2 - q^2}$

Rastall theory of gravity is studied by using the GYOTO code. The shadow cast by the KNNK black hoe in the Rastall theory of gravity with the use of the TM code is done in the Sect. 5. A discussion of the work done is presented in the last section.

2 Kerr–Newman–NUT–Kiselev spacetime in the Rastall gravity

The spacetime around the KNNK black hole in the RG is described by the metric (see [37])

$$\begin{aligned} ds^2 = &-\frac{\Delta}{\rho^2}[\mathrm{d}t - \{a\sin^2\theta + 2l(1-\cos\theta)\}\mathrm{d}\phi]^2 \\ &+\frac{\rho^2}{\Delta}\mathrm{d}r^2 + \rho^2\mathrm{d}\theta^2 + \frac{\sin^2\theta}{\rho^2}[a\mathrm{d}t - \{r^2+(a+l)^2\}\mathrm{d}\phi]^2, \end{aligned} \tag{1}$$

where

$$\Delta = r^2 - 2Mr + a^2 + e^2 + g^2 - l^2 - \alpha r^{\upsilon}, \tag{2}$$

$$\upsilon = \frac{1-3\omega}{1-3\kappa\lambda(1+\omega)}, \tag{3}$$

$$\rho^2 = r^2 + (l + a\cos\theta)^2, \tag{4}$$

and, M and a are the gravitational mass and specific angular momentum of the black hole, respectively. The rest of the parameters related to the KNNK black hole in the RG are: l is the gravitomagnetic charge or so-called NUT parameter, α is the quintessential intensity, $\kappa\lambda$ is the Rastall gravity parameter, ω_q is the parameter of equation of state of the quintessence, e and g are related to the electric and magnetic charges of the black hole, respectively [37]. New parameter $q^2 = e^2 + g^2$ is introduced to take into account the contribution of the electric and magnetic charges of the KNNK black hole in the RG to the spacetime properties.

The KNNK black hole in RG may have several horizons depending on the values of the parameters ω_q and $\kappa\lambda$. The event horizons are determined as the coordinate singularity of the spacetime and as a null hypersurface of constant r. Consequently, the event horizons are defined as the roots of the following algebraic equation

$$r^2 - 2Mr + a^2 + q^2 - l^2 - \alpha r^{\upsilon} = 0. \tag{5}$$

The horizon coincides to have only inner and outer parts or there is no cosmological horizon for the selected values of the parameters ω_q and $\kappa\lambda$. The thermodynamic properties of black holes can be easily explored in this specific case of the horizon. Due to this reason only two roots for the horizon are explored in [51]. It is difficult to study, for example, the entropy product in case of existence of more than two roots of the horizon equation due to more complicated computations. In [37], the circumstances when there will be two analytic roots are explored and collected in the Table 1.

3 Thin accretion disk model

According to the Novikov–Thorne model [12], accretion disk formed around the central KNNK black hole in the RG is geometrically thin but optically it is thick. The vertical size or the height of the thin accretion disk is always considered negligible as compared to the horizontal size or spread of the accretion disk. In other words, the maximum half thickness (height h) of the accretion disk in the vertical direction is always much smaller than the characteristic radius r of the disk in the horizontal direction, consequently $h \ll r$. In the accreting matter the pressure gradient and gradient of a vertical entropy are both negligible due to hydrodynamic equilibrium in a thin accretion disk. The efficient cooling through the thermal radiation over surface of the whole disk prevents disk from simulation of the heat produced by stresses and dynamical friction. This equilibrium stabilizes thin vertical size of the accretion disk. Consequently, in the higher orbits the accreting plasma is in a typical Keplerian motion and an inner edge of the thin accretion disk is at the marginally stable orbit around the compact object.

For steady state accretion disk models the mass accretion rate $\dot{M}_0$ does not depend on time. The physical quantities averaged over a characteristic time scale, e.g. Δt, for a total period of the orbits over the azimuthal angle $\Delta\phi = 2\pi$ and over the vertical height h, describe the orbiting plasma [6, 7, 12]. For a particle with mass m orbiting the central KNNK black hole in the RG at the equatorial plane the effective potential can be written as [7, 12, 52]

$$V_{\rm eff}(r) = -1 + \frac{E^2 g_{\phi\phi} + 2EL g_{t\phi} + L^2 g_{tt}}{g_{t\phi}^2 - g_{tt} g_{\phi\phi}} \,, \tag{6}$$

where the conserved quantities E and L are the specific energy and the specific angular momentum of a particle, respectively. These two constants of motion can be expressed through the components of the metric tensor as

$$E = -\frac{g_{tt} + \Omega g_{t\phi}}{\sqrt{-g_{tt} - 2\Omega g_{t\phi} - \Omega^2 g_{\phi\phi}}} \,, \tag{7}$$

and

$$L = \frac{\Omega g_{\phi\phi} + g_{t\phi}}{\sqrt{-g_{tt} - 2\Omega g_{t\phi} - \Omega^2 g_{\phi\phi}}} \,, \tag{8}$$

and the angular velocity is

$$\Omega = \frac{{\rm d}\phi}{{\rm d}t} = \frac{-g_{t\phi,r} \pm \sqrt{\{-g_{t\phi,r}\}^2 - \{g_{\phi\phi,r}\}\{g_{tt,r}\}}}{g_{\phi\phi,r}} \,. \tag{9}$$

The inner edge of the thin accretion disk around central KNNK black hole in the RG coincides with the inner most stable circular orbit (ISCO) of test particles orbiting the KNNK BH in the RG in the chosen model. A solution of the following set of conditions on the effective potential of the test particle

$$V_{\rm eff}(r) = 0 \,, \quad V'_{\rm eff}(r) = 0 \,, \quad V''_{\rm eff}(r) = 0 \,, \tag{10}$$

provides the position of the inner edge of the thin accretion disk around the central KNNK black hole in the RG.

The accretion disk emits the electromagnetic radiation with the total flux [7, 12]

$$F(r) = -\frac{\dot{M}_0 c^2}{4\pi M^2} \frac{\Omega_{,r}}{\sqrt{-g}(E - \Omega L)^2} \int_{r_{ISCO}}^{r} (E - \Omega L) L_{,r} {\rm d}r, \tag{11}$$

where g is the determinant of the metric tensor. For the selected values of the spacetime parameters, the radial dependence of the flux of the radiant energy over the accretion disk is presented in Fig. 1, containing two upper and bottom panels. From the upper and bottom panels, one can see that increase of the parameter α essentially reduces the flux of the accretion disk. This behavior justifies that the quintessential intensity has strong impact on the gravitational field of KNNK black hole in the RG. Moreover, it is observed that increase of this parameter shifts the lines outwards the central object indicating that for the bigger values of the parameter α, we would get bigger ISCO location which in turn defines the inner edge of the accretion disk around the KNNK black hole in the RG. One can also see that for smaller values of the parameter ω_q the maximum value of the flux also decreases while for the far distances this change is negligible. One can also notice a small increase in the values of the flux for the smaller values of the parameter $\kappa\lambda$ as it can be easily seen from the set of the graphs in the bottom panel of the Fig. 1.

The radial profile of the temperature of the accretion disk of the KNNK black hole in the RG is demonstrated in Fig. 2 based on the assumption that the flux of the accretion disk is expressed as $F = \sigma T^4$ corresponding to the black body radiation where σ is the Boltzmann constant. It is demonstrated that the temperature of the disk is higher when the quintessential intensity takes smaller values. It is also shown that for bigger values of the parameter ω_q one would get higher temperature of the disk in the close environment of the central black hole. While for the far distances the temperature becomes higher for the smaller values of this parameter being opposite to the behavior of the lines for the different values of the parameter $\kappa\lambda$. Again, we observe that the quintessential intensity has much stronger influence on the behavior of the lines compared to the other parameters as we have seen in the previous paragraph.

4 Black hole shadow obtained using GYOTO code

GYOTO is an open ray-tracing code [28], and based on the suggestion that a black hole is surrounded by enough objects (e.g. accretion disk) which can emit light rays. The observer at the infinity can receive the rays in order to get the information of the black hole and the surrounding matter around the black hole.

The original code of the geometrically thin infinite accretion disk in GYOTO describes the Schwarzschild and Kerr spacetimes. In order to describe other spacetimes one needs to modify the code accordingly. The main modification of the code for our case contains two major changes: (i) to change the spacetime metric from the Kerr one to the KNNK spacetime metric in the RG; (ii) to

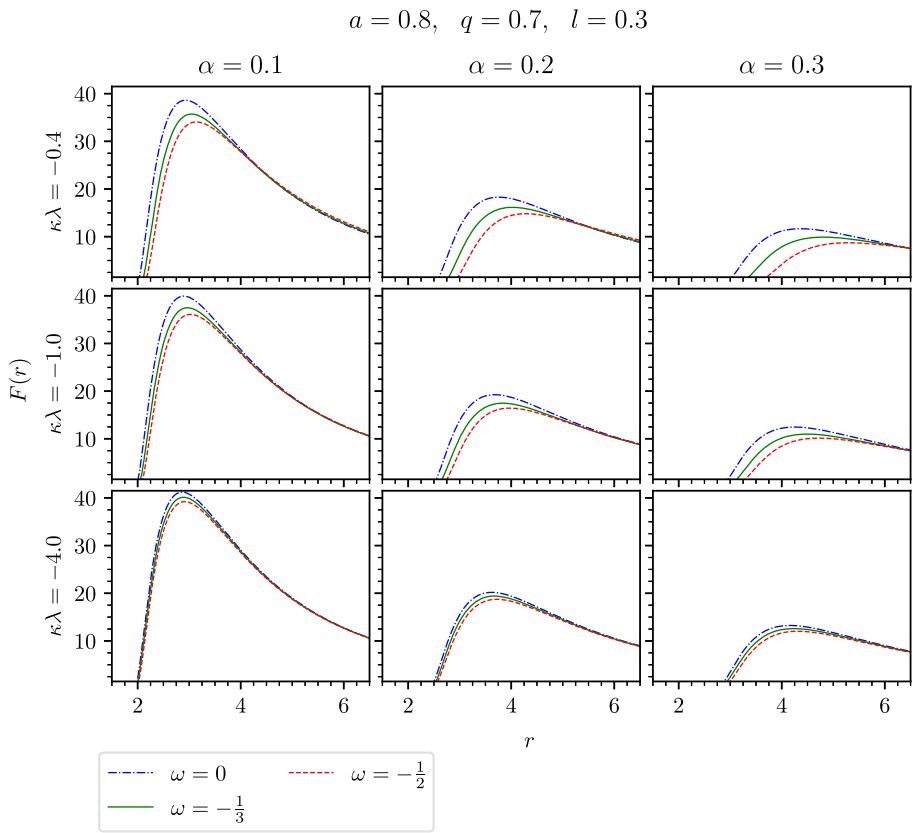

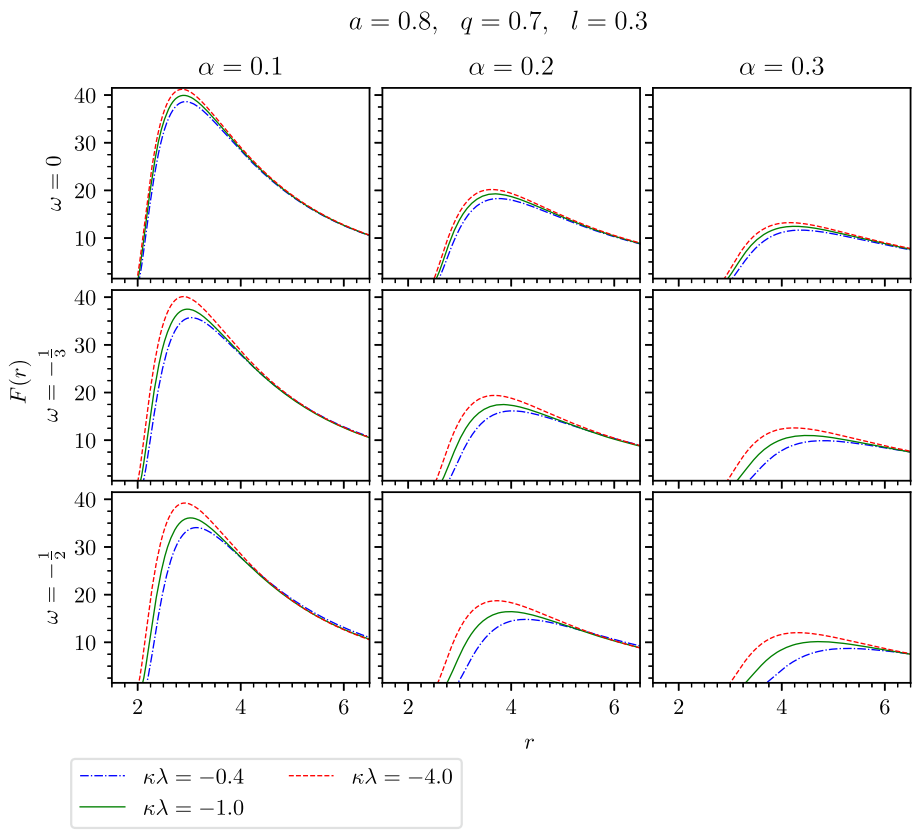

Fig. 1 The radial dependence of radiant flux of the accretion disk around the KNNK black hole in the RG for different values of the spacetime parameters. For the top panel, each row has different value for the parameter ω_q. For the bottom panel, each row has different value for the parameter $\kappa\lambda$

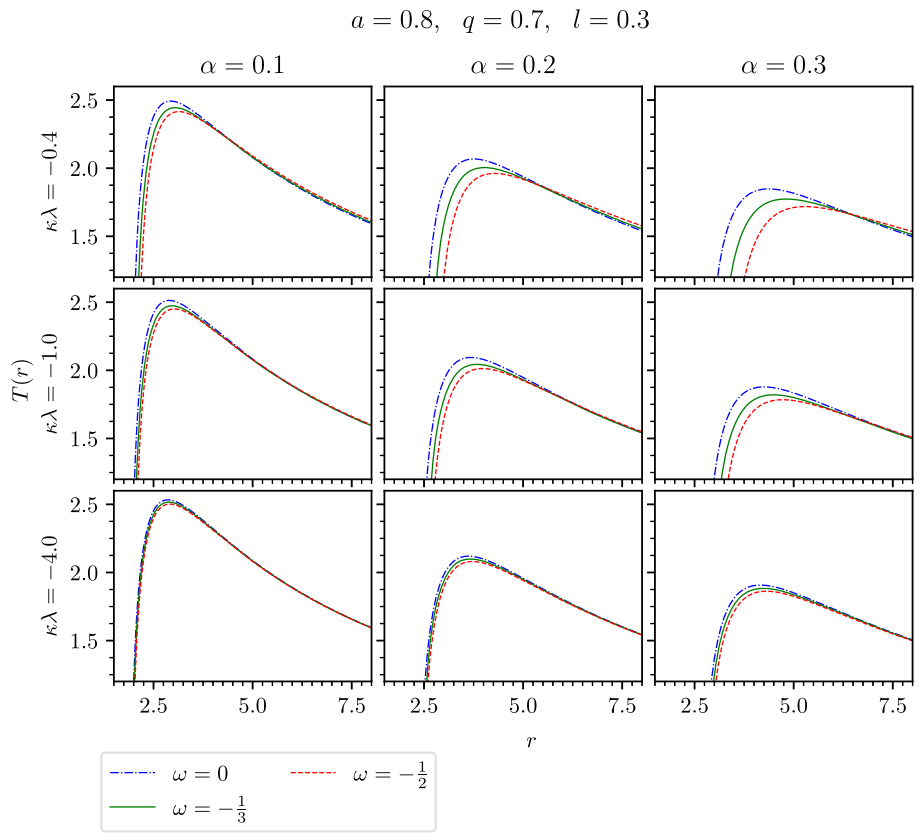

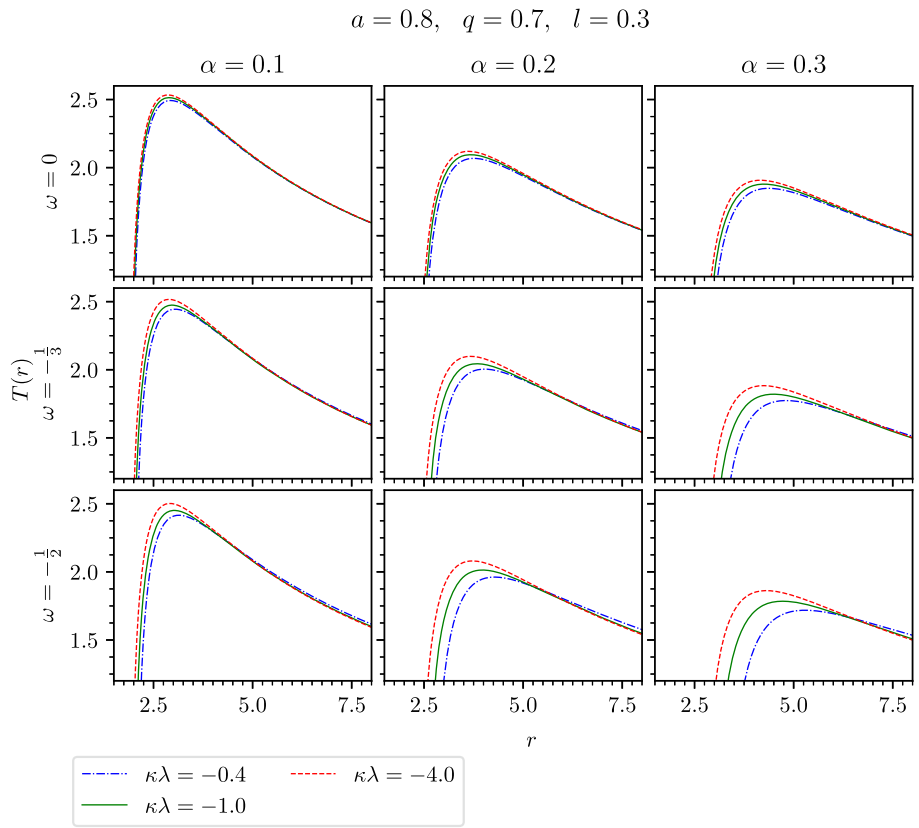

Fig. 2 Temperature profile of the accretion disk around central KNNK black hole in the RG for different values of the spacetime parameters. For the top panel each row has different value for the parameter $\kappa\lambda$. For the bottom panel each row has different value for the parameter ω_q

change the equation of motion. The first change is easy to implement while the second one is a bit tedious. Below we describe the modifications of the GYOTO code due to the change of equation of motion.

Using the Hamiltonian formulation one can express the Lagrangian $\mathcal{L}$ and the momentum p^α in the following form:

$$\mathcal{L} = \frac{1}{2} g_{\alpha\beta} \dot{q}^\alpha \dot{q}^\beta,$$

$$p^\alpha \equiv \dot{q}^\alpha, \tag{12}$$

$$p_\alpha \equiv \frac{\partial \mathcal{L}}{\partial \dot{q}^\alpha} = g_{\alpha\beta} \dot{q}^\beta = g_{\alpha\beta} p^\beta. \tag{13}$$

The covariant and contravariant components of the momentum can be related as:

$$\begin{aligned} p_t &= g_{tt} p^t + g_{t\phi} p^\phi \ , \\ p_r &= g_{rr} p^r \ , \\ p_\theta &= g_{\theta\theta} p^\theta \ , \\ p_\phi &= g_{\phi\phi} p^\phi + g_{\phi t} p^t \ . \end{aligned} \tag{14}$$

Now one can define the Hamiltonian in the following standard way:

$$H = p_\mu \dot{q}^\mu - \mathcal{L} = \frac{1}{2} g^{\alpha\beta} p_\alpha p_\beta \ . \tag{15}$$

Through Hamilton's equations:

$$\dot{q}_i = \frac{\partial H}{\partial p_i} \quad , \quad \dot{p}_i = -\frac{\partial H}{\partial q_i} \ , \tag{16}$$

one can easily express the equations of motion (with $E = -p_t$ and $L = -p_\phi$):

$$\dot{r} = g^{rr} p_r \ , \tag{17}$$

$$\dot{p}_r = -\frac{1}{2}(g^{tt})' E^2 - \frac{1}{2}(g^{rr})' {p_r}^2 - \frac{1}{2}(g^{\theta\theta})' {p_\theta}^2 \tag{18}$$

$$-\frac{1}{2}(g^{\phi\phi})' L^2 - (g^{t\phi})' EL \ , \tag{19}$$

$$\dot{\theta} = g^{\theta\theta} p_\theta \ , \tag{20}$$

$$\dot{p}_\theta = -\frac{1}{2}(g^{tt})^\star E^2 - \frac{1}{2}(g^{rr})^\star {p_r}^2 - \frac{1}{2}(g^{\theta\theta})^\star {p_\theta}^2 \ , \tag{21}$$

$$-\frac{1}{2}(g^{\phi\phi})^\star L^2 - (g^{t\phi})^\star EL \ , \tag{22}$$

$$\dot{t} = g^{tt} E \ , \tag{23}$$

$$\dot{p}_t = 0 \ , \tag{24}$$

$$\dot{\phi} = g^{\phi\phi} L \tag{25}$$

$$\dot{p}_\phi = 0 \ , \tag{26}$$

where the superscripts $'$ and $\star$ denote differentiation with respect to r and θ, respectively.

It is worth to mention that the equation of the emitted flux we used is same as Eq. (11) and has the following form [28]:

$$I_\nu \propto \frac{1}{(\rho^2 - 3)\rho^5} \left\{ \rho - \frac{3}{\sqrt{2}} \ln \left[(3 - 2\sqrt{2}) \frac{\rho + \sqrt{3}}{\rho - \sqrt{3}} \right] \right\} , \tag{27}$$

where the $\rho = \sqrt{r/M}$.

The accretion disk in GYOTO does not have the bottom region which can be explained in the following content. The Fig. 3 shows two different types of photon orbits in the accretion disk. In each figure, four points (A, B, C and D) correspond to the emission source around the accretion disk. In Fig. 3a the four points (A, B, C and D) emit light rays which are bent by the black hole and finally captured by the observer. In this figure the light rays do not cross each other, so one may call them uncrossed orbits. In Fig. 3b the same four points (A, B, C and D) as in Fig. 3a emit light rays but the light rays cross another light ray, so one may call them crossed orbits.

The different types of photon orbits in the accretion disk will form different regions of the accretion disk as shown in Fig. 4a. The uncrossed orbits (Fig. 3a) form the upper region as shown in Fig. 4a with the blue colour. The bottom region is formed by the crossed orbits (Fig. 3b) as shown in Fig. 4a with green colour. In Fig. 4 we show the accretion disk of the Schwarzschild black hole

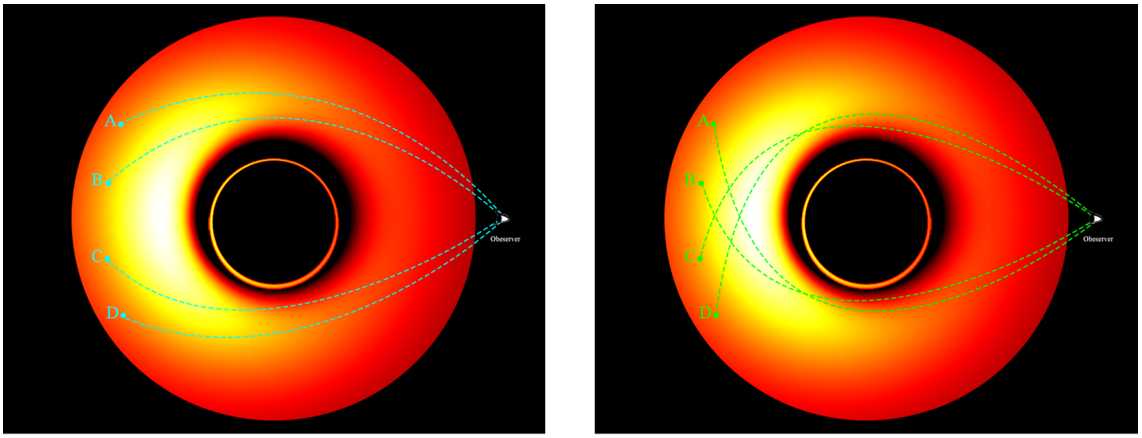

(a)Uncrossed orbits (b)Crossed orbits

Fig. 3 Different photon orbits in the accretion disk. The photon orbits in left figure do not cross but in right figure they cross

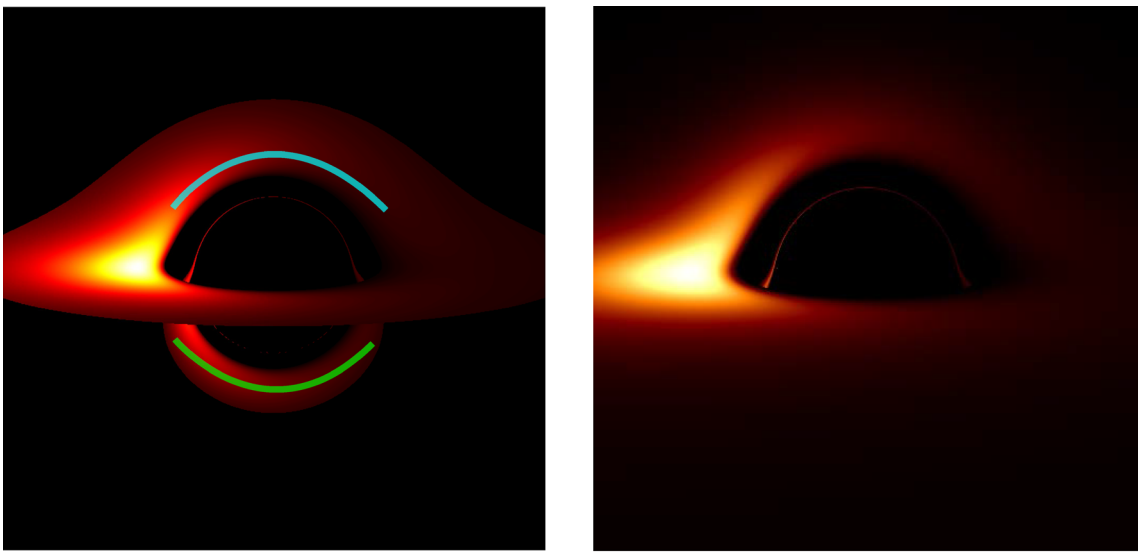

(a)Full Accreting disk (b)Gyoto's Accreting disk

Fig. 4 The accretion disk of the Schwarzschild black hole illustrated using two different codes. The left figure is the accretion disk generated using TM code, the right one is the accretion disk generated using GYOTO

with inclination angle equal to 80°. The right figure is from the GYOTO code, and the left figure is from the TM code. Through this figure one can see that GYOTO only considers the uncrossed orbits when calculating the accretion disk. Particularly, in [53], the images are similar to the one shown in Fig. 4b are called direct images of the disk

In Fig. 5 we get the accretion disk from GYOTO for the fixed values of $a = 0.80$, $q = 0.70$, $l = 0.30$ and observation angle $\theta = 80°$. The upper plots in Fig. 5, correspond to the fixed value of $\omega = -1/2$ and for different values of $\kappa\lambda(-0.4, -1.0$ and $-4.0)$ and α (0.10, 0.20 and 0.30). The lower plots in Fig. 5 correspond to the fixed value of $\kappa\lambda = -0.4$ and for the different values of $\omega_q(0, -1/3$ and $-1/2)$ and $\alpha(0.10, 0.20$ and $0.30)$. From the first row in the upper plots of Fig. 5 one can observe that with the increase of α the area of the shadow of the black hole will increase. The second and third rows show that with the increase of $\kappa\lambda$ the area of the shadow of the black hole increases intensively. From the first column in the upper plots of Fig. 5 one can see that with the increase of $\kappa\lambda$ the area of the shadow of the central black hole will increase. The second and third columns show that with the increase of α the area of the black hole shadow increases intensively. From the first row in the lower plots of Fig. 5 one can observe that with the increase of α the area of the shadow of the black hole will increase. The second and the third rows show that with the increase of ω_q the area of the shadow of the black hole increases intensively. From the first column in the lower plots of Fig. 5 one can see that with the increase of ω_q the area of the shadow cast by the black hole twill decrease. The second and third columns show that with the increase of α the area of black hole shadow increases intensively.

In Fig. 6 we get the accretion disk from GYOTO code for the fixed values of $a = 0.80$, $q = 0.70$, $l = 0.30$ and of the observation angle $\theta = 45°$. The upper plots correspond to the fixed value of $\omega = -1/2$ and for the different values of $\kappa\lambda(-0.4, -1.0$ and $-$

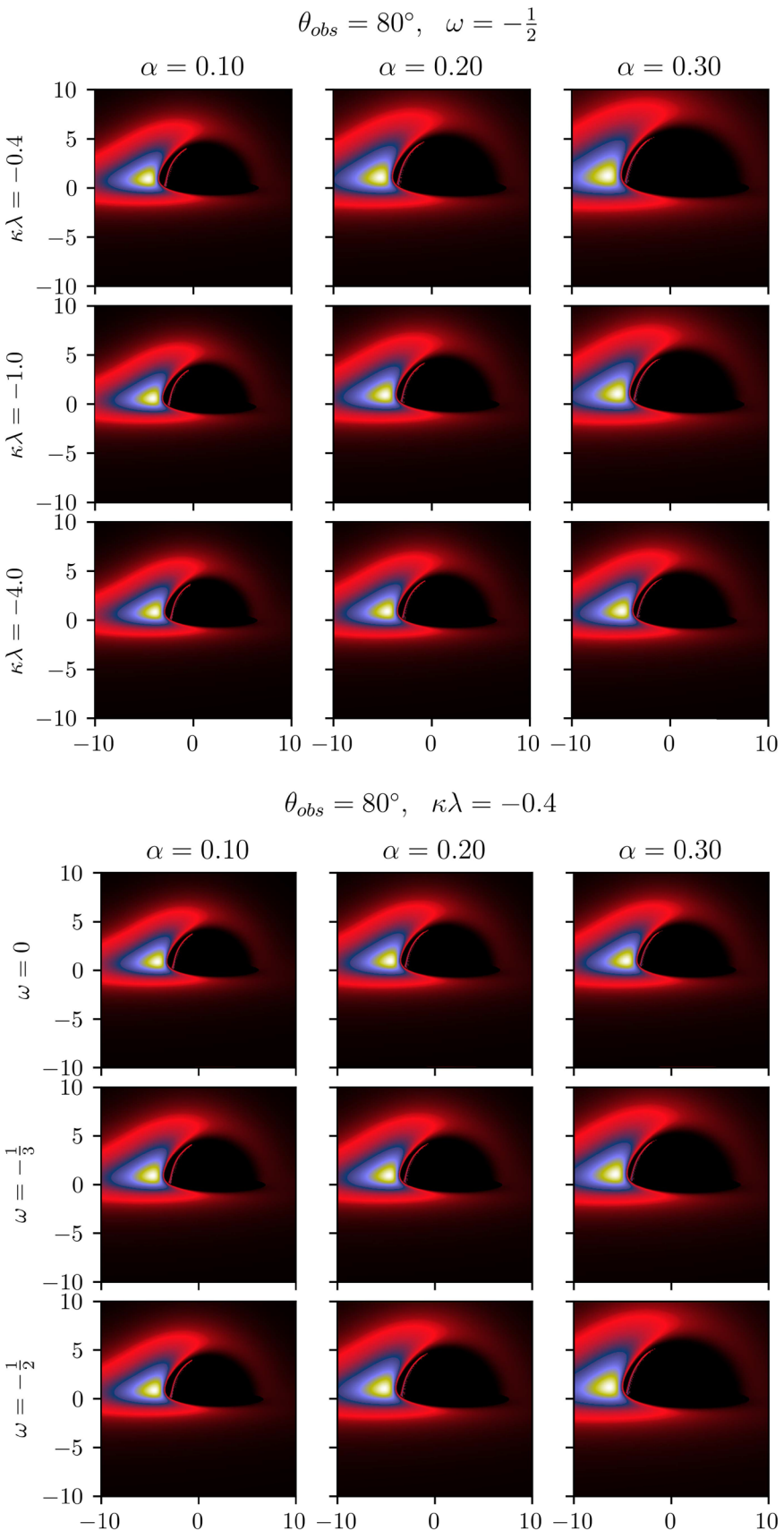

Fig. 5 The accretion disk generated using GYOTO code for the fixed values of $a = 0.80$, $q = 0.70$, $l = 0.30$ and observation angle $\theta = 80°$. The upper plots correspond to the fixed value of $\omega = -1/2$ and for the different values $\kappa\lambda$ ($-$ 0.4, $-$ 1.0 and $-$ 4.0) and α(0.10, 0.20 and 0.30); the lower plots correspond to the fixed value of $\kappa\lambda = -0.4$ and for the different values of ω_q (0, $-$ 1/3 and $-$ 1/2) and α(0.10, 0.20 and 0.30)

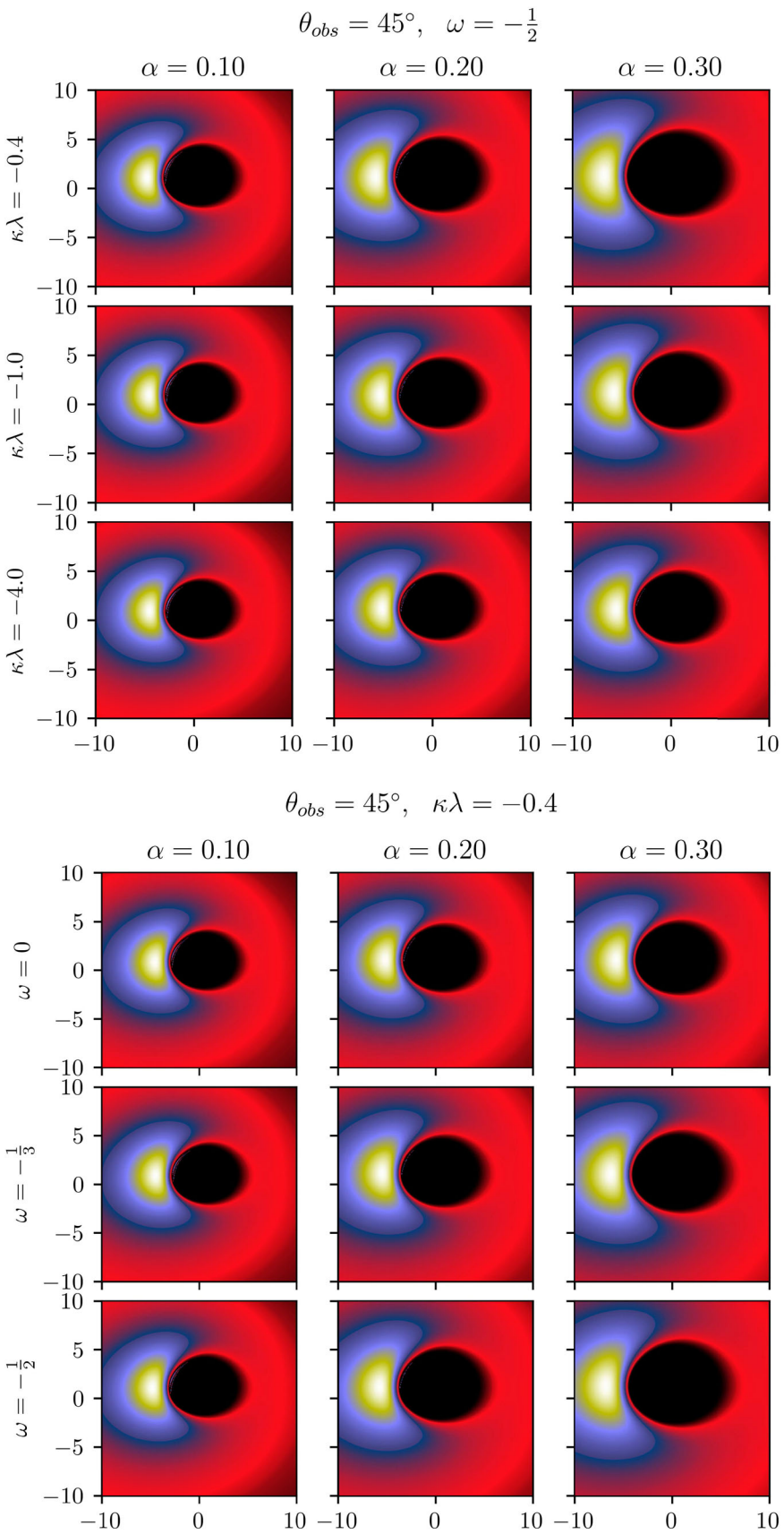

Fig. 6 The accretion disk generated using GYOTO code for the fixed values $a = 0.80$, $q = 0.70$, $l = 0.30$ and observation angle $\theta = 45°$. The upper plots correspond to the fixed value $\omega = -1/2$ and for the different values $\kappa\lambda(-0.4, -1.0$ and $-4.0)$ and $\alpha(0.10, 0.20$ and $0.30)$; the lower plots correspond to the fixed value of $\kappa\lambda = -0.4$ and for the different values of $\omega_q(0, -1/3$ and $-1/2)$ and $\alpha(0.10, 0.20$ and $0.30)$

4.0) and α(0.10, 0.20 and 0.30). The lower plots in the Fig. 6 correspond to the fixed value of $\kappa\lambda = -0.4$ and for the different values of ω_q(0, − 1/3 and − 1/2) and α(0.10, 0.20 and 0.30). One may see similar results as shown in Fig. 5: α and $\kappa\lambda$ will increase the shadow cast by the KNNK black hole and also the rate of increase. The parameter ω_q will decrease the shadow size of the black hole and also the rate of decrease. In Fig. 7 we get the accretion disk from the GYOTO code for the fixed value of $a = 0.80$, $q = 0.70$, $l = 0.30$ and of the observation angle $\theta = 45°$. The upper plots of the Fig. 7 correspond to fixed value of $\omega = -1/2$ and for different values of $\kappa\lambda$(− 0.4, − 1.0 and − 4.0) and α(0.10, 0.20 and 0.30). The lower plots of the same Fig. 7 correspond to fixed value of $\kappa\lambda = -0.4$ and for the different values of ω_q(0, − 1/3 and − 1/2) and α(0.10, 0.20 and 0.30). We observe the similar results as shown in Figs. 5 and 6.

5 Development of the TM code to obtain black hole shadow

Ray tracing technique is used to simulate imaginary rays of light sent from the observer to the object, in three-dimensional space. The C,C++ and Python programming languages are used to create this code. The code algorithm consists of processing all possible trajectories which may exist in black hole environment [29–31].

5.1 Black hole shadow

The determination of the geometrical structure of the black hole shadow consists of several steps described below.

1. Determination of initial conditions of the photon assuming the position of the detected photon in the screen. The following basic expressions [54]

$$r_i = \left(d^2 + \bar{\alpha}^2 + \bar{\beta}^2\right)^{1/2}, \tag{28}$$

$$\theta_i = \arccos\left(\frac{d\cos\theta_{\rm obs} + \bar{\beta}\sin\theta_{\rm obs}}{r_i}\right), \tag{29}$$

$$\phi_i = \arctan\left(\frac{\bar{\alpha}}{d\sin\theta_{\rm obs} - \bar{\beta}\cos\theta_{\rm obs}}\right), \tag{30}$$

and

$$\left(\frac{{\rm d}r}{{\rm d}\lambda'}\right)_i = \frac{d}{r_i}, \tag{31}$$

$$\left(\frac{{\rm d}\theta}{{\rm d}\lambda'}\right)_i = \frac{-\cos\theta_{\rm obs} + \frac{d}{r_i^2}(d\cos\theta_{\rm obs} + \bar{\beta}\sin\theta_{\rm obs})}{\sqrt{r_i^2 - (d\cos\theta_{\rm obs} + \bar{\beta}\sin\theta_{\rm obs})^2}}, \tag{32}$$

$$\left(\frac{{\rm d}\phi}{{\rm d}\lambda'}\right)_i = \frac{-\bar{\alpha}\sin\theta_{\rm obs}}{\bar{\alpha}^2 + (d\cos\theta_{\rm obs} + \bar{\beta}\sin\theta_{\rm obs})^2}, \tag{33}$$

$$\left(\frac{{\rm d}t}{{\rm d}\lambda'}\right)_i = -\left[g_{rr}\left(\frac{{\rm d}r}{{\rm d}\lambda'}\right)_i^2 - g_{\theta\theta}\left(\frac{{\rm d}\theta}{{\rm d}\lambda'}\right)_i^2 - g_{\phi\phi}\left(\frac{{\rm d}\phi}{{\rm d}\lambda'}\right)_i^2\right]^{1/2}, \tag{34}$$

   are used to determine the initial position and the four-momentum of each photon. Here, d is the distances from the observer to the black hole, $\bar{\alpha}$ and $\bar{\beta}$ are the celestial coordinates in the observer's sky and $\theta_{\rm obs}$ is the inclination angle.
2. Numerical solution of the equation of motion. Geodesic equations

$$\frac{{\rm d}^2x^\mu}{{\rm d}s^2} + \Gamma^\mu_{\alpha\beta}\frac{{\rm d}x^\alpha}{{\rm d}s}\frac{{\rm d}x^\beta}{{\rm d}s} = 0, \tag{35}$$

   with

$$\Gamma^\beta_{\alpha\nu} = \frac{1}{2}g^{\mu\beta}\left(\partial_\alpha g_{\mu\nu} + \partial_\nu g_{\mu\alpha} - \partial_\mu g_{\alpha\nu}\right),$$

   $\Gamma^\beta_{\alpha\nu}$ as the Christoffel symbols are applied to determine the equations of motion of a photon.
3. Determination of photon trajectory.
4. Selection of photons whose trajectories most closely approach to the black hole and do not fall inside the region of the event horizon.
5. Construction of the shadow structure based on the positions of the light rays of the selected photons in the screen as described in item 4.

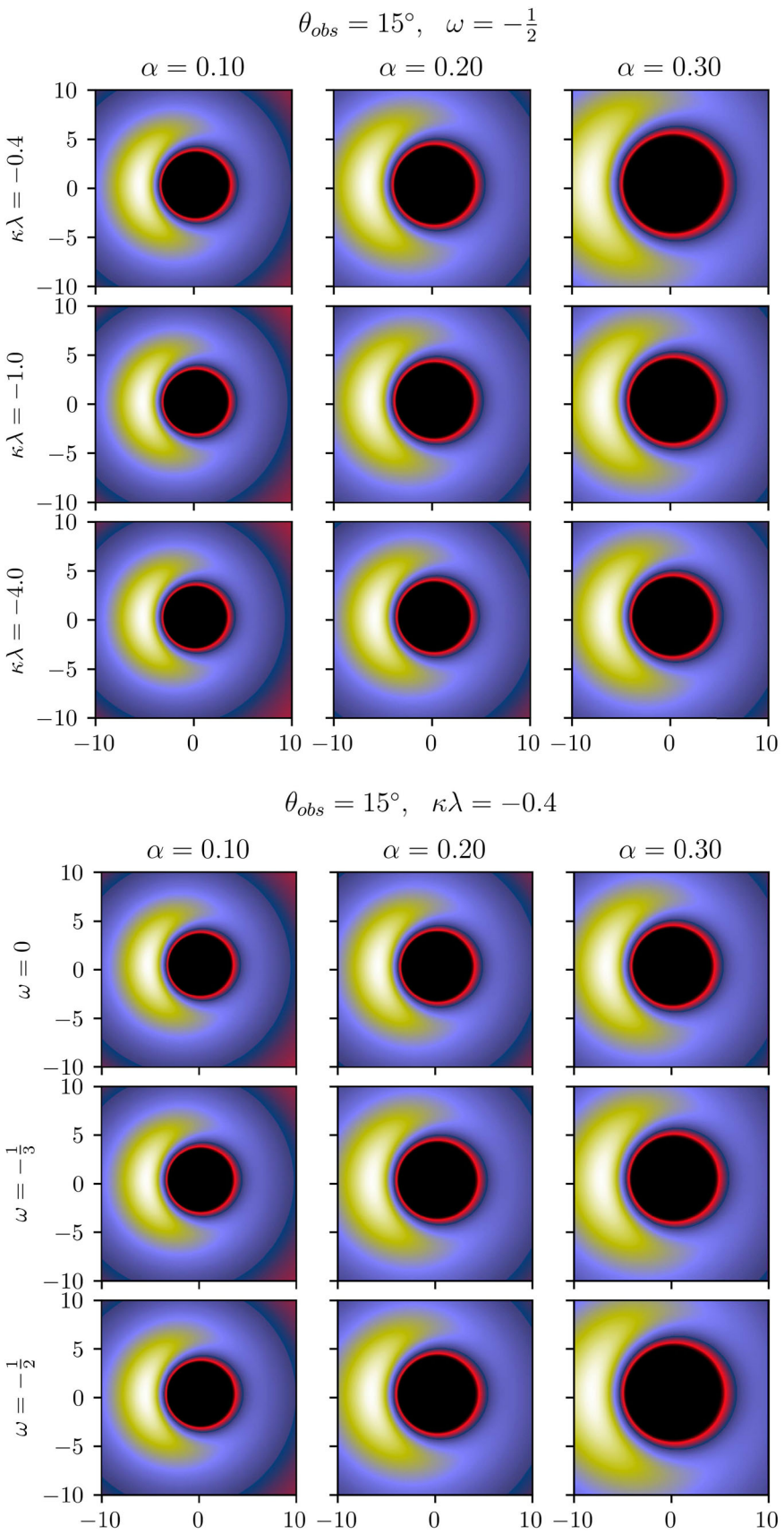

Fig. 7 The accretion disk generated using GYOTO code for the fixed values of $a = 0.80$, $q = 0.70$, $l = 0.30$ and observation angle $\theta = 15°$. The upper plots correspond to the fixed value $\omega = -1/2$ and for different values of $\kappa\lambda(-0.4, -1.0$ and $-4.0)$ and $\alpha(0.10, 0.20$ and $0.30)$; lower plots correspond to the fixed value of $\kappa\lambda = -0.4$ and for the different values of $\omega_q(0, -1/3$ and $-1/2)$ and $\alpha(0.10, 0.20$ and $0.30)$

5.2 Black hole accretion disk

Ray tracing code allows to determine the shadow of a black hole, and in addition is powerful tool to get an image of its accretion disk. We will use here the well known Novikov–Thorne model [12] of a thin accretion disk. According to this model the radiation energy flux of the accretion disk of the black hole is determined by using Eq. (11).

The algorithm for numerical solution of the given problem consists of the following steps:

1. Determining the initial conditions of the photon considering the position of the photon being fixed in the screen.
2. Numerical solution of the equations of photon's motion;
3. Determination of photons trajectory.
4. Selection of photons. Selected photons have to meet the following conditions and criteria:
   (a) the photon trajectory does not intersect the event horizon;
   (b) photons trajectories have to cross the accretion disk
5. If the condition 4(b) is satisfied, we keep the position of inter-crossing with the disk and the initial conditions of the corresponding photon.

We calculate the energy flux of radiation for the position found according to the statement (5) using Eq. (11). We display the results of the performed calculations in the form of color-map as in Figs. 8, 9, and 10 for different inclination angles and values of the spacetime parameters we are interested in. It is worth noting that in the figures the frequency of photons has tendency to be increased with the change of the color from red to white (black parts determine the regions where photons are absent) due to the well-known Doppler effect. Figure 8 indicates the appearance of close environment of a black hole as it is seen by a distant observer being far away from the gravitating object containing thin accretion disk when the inclination angle is fixed to be $\theta_{\rm obs} = 80^\circ$. The black region in the center defines the shadow formed due to the capture and bending of photons by the central black hole. We will explore the shadow in a detailed way latter but even here one can clearly observe that the size of the shadow of the black hole is strongly affected by the quintessential intensity and is enlarged for bigger values of the latter. One can also see that the change of the shadow size with the change of parameters $\kappa\lambda$ and ω_q becomes noticeable only for the bigger values of the parameter α. It appears that the left part (with respect to the central black hole) of each panel is brighter than the right part. This is due to the fact that particles moving around the central black hole and forming the accretion disk are assumed to have retrograde motion so particles in the left correspond to the ones approaching the observer while the particles in the right to the ones receding the observer. Since the frequency of photons approaching the observer is higher than the frequency of the receding ones due to the Doppler beaming effect, the left hand side of the pictures looks brighter than the right hand side. Figures 9 and 10 represent the appearance of the central black hole with accretion disk for the inclination angles 45° and 15°, respectively, and can be interpreted in the same way as in the previous case. The case of $\theta_{\rm obs} = 15^\circ$ is especially interesting as it has the inclination angle being close to the one for the black hole source M87 observed by EHT consortium [55, 56], and one can see that the given pictures indeed represent the image obtained observationally.

Now, we study the change of the shape and size of the shadow formed around the KNNK black hole in the RG in a more detailed way as a continuation of the discussion done in the previous paragraph. The shape of the black hole shadow is presented as the curved closed lines in the Figs. 11, 12, and 13 for the selected values of the inclination angle and the spacetime parameters. It can be observed that the increase of the parameter α considerably enlarges the size of the shadow of the KNNK black hole in the RG when the parameter $\kappa\lambda$ takes bigger values and ω_q takes smaller values. It was stated in the previous paragraph that for the bigger values of the parameter α the change of the shadow size with the change of $\kappa\lambda$ and ω_q is considerable and one can now clearly observe this phenomena from the figures presented here. One can see that when $\kappa\lambda = -0.4$ the change of the shadow cast by the KNNK black hole in the RG with the change of the rest two spacetime parameters is negligible. Similar behavior of the shadow of the central black hole can be observed when $\omega = 0$. Now one can clearly observe that the change of the shadow size with the change of α is noticeable only when $\kappa\lambda$ is close to 0 and ω_q is smaller than 0. One can also notice from the figures that the position of the center of the shadow of the black hole and its shape strongly depend on the inclination angle at what the observer looks to the central black hole. It is demonstrated that the center of the shadow coincides with the center of the black hole for smaller values of the inclination angle and shifts towards the right side when one increases the angle. As for the shape of the shadow one can observe that it takes circle-like form for smaller inclination angles and becomes more deformed for bigger values of the inclination angle.

6 Discussion

In this work we have explored the spacetime around the KNNK black hole in the RG to study the effects of strong gravitational field on the light rays emitted from the particles in the accretion disk formed around the central black hole. We have used the thin accretion disk model of Novikov and Thorne in our study. We have shown that the observed thermal flux of the thin accretion disk strongly depends on the quintessential intensity of the KNNK black hole in the RG. We have observed that the thermal flux of the accretion disk decreases for the bigger values of the quintessential intensity parameter α. We have also observed that the thermal flux of the accretion disk has reduced for comparatively smaller values of the parameter ω_q, and this effect is more considerable when

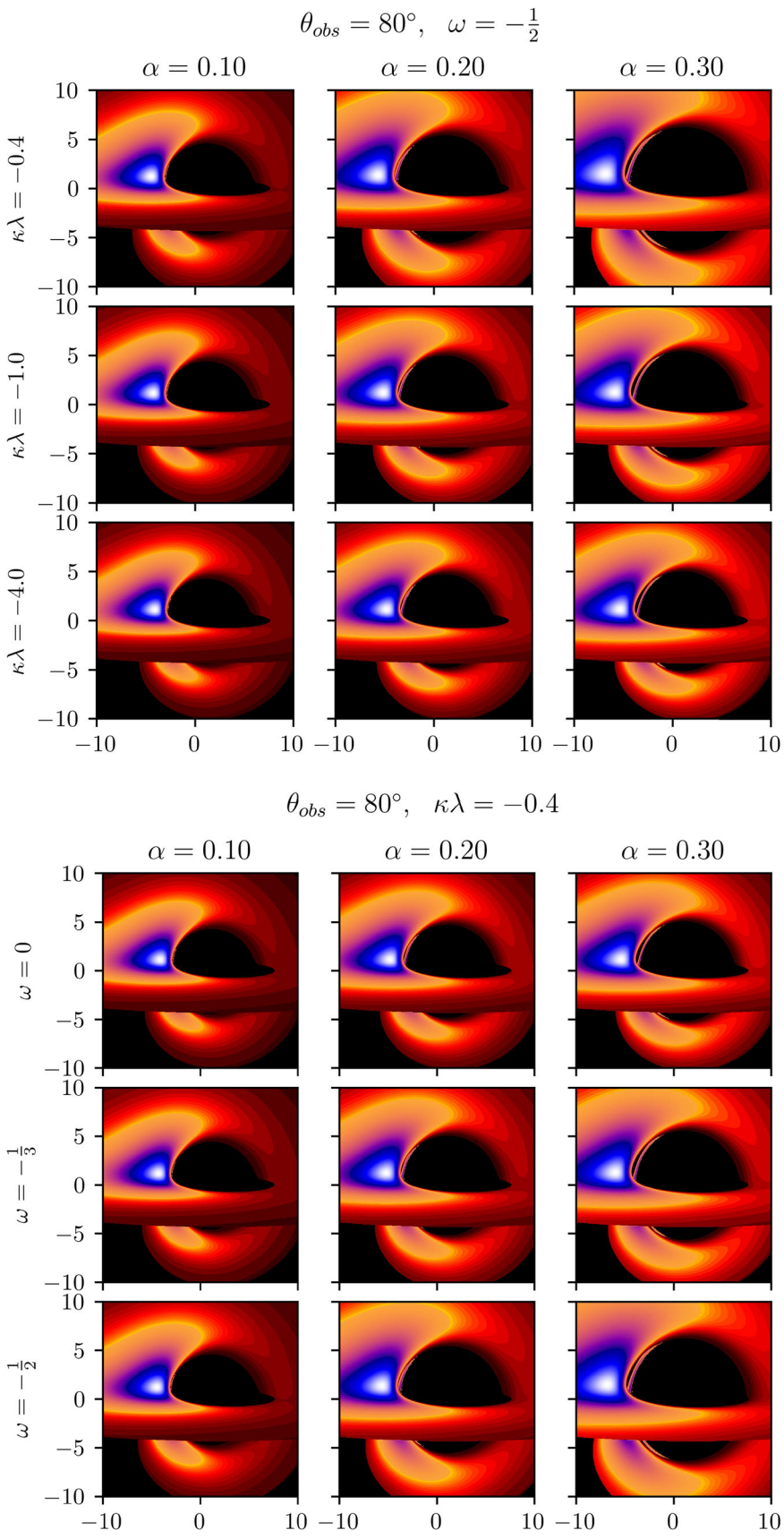

Fig. 8 The simulated image of the accreting disk from the TM code for $\theta = 80°$. The values of spacetime parameters are taken as in Fig. 5

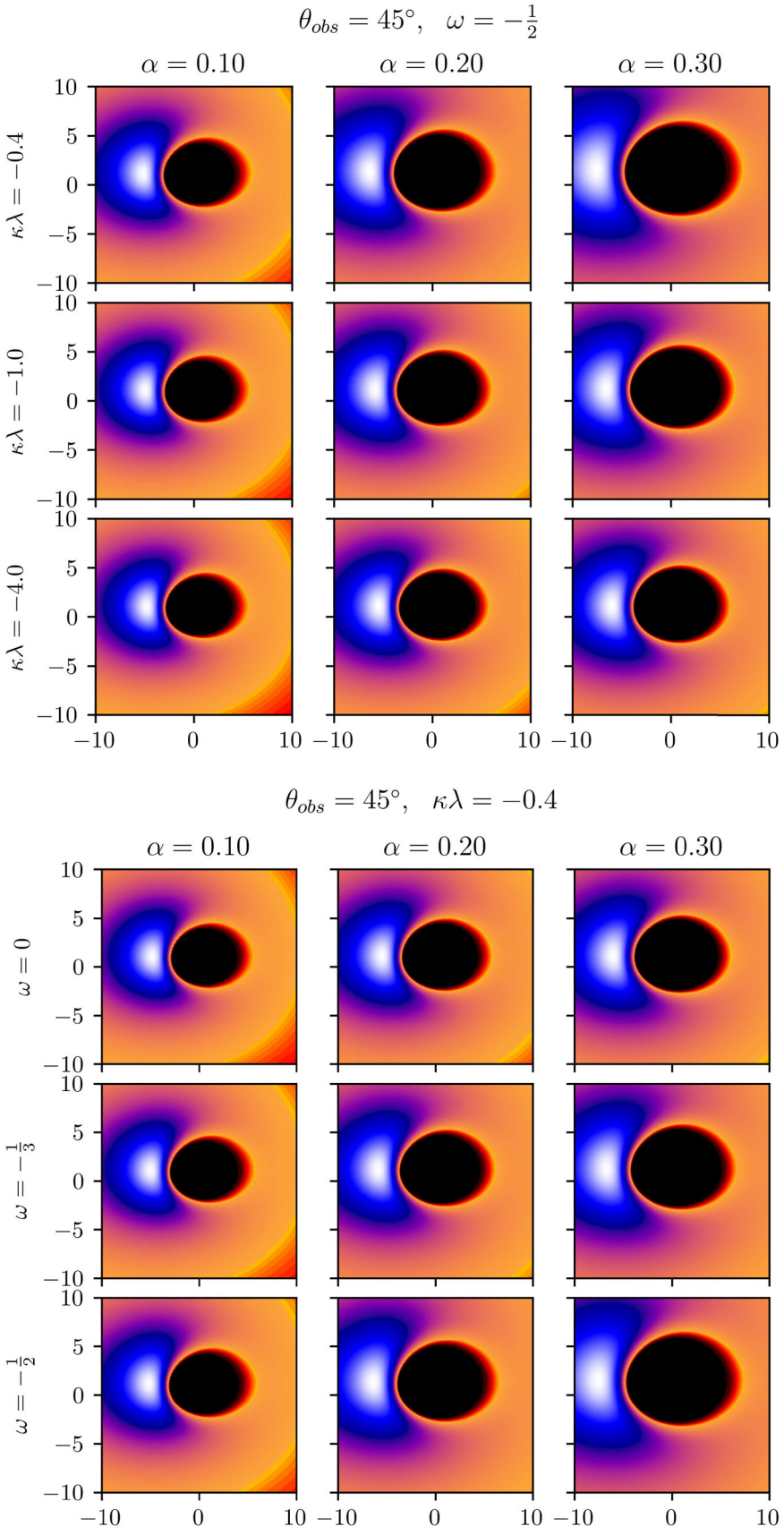

Fig. 9 The same as Fig. 8 but for $\theta = 45°$

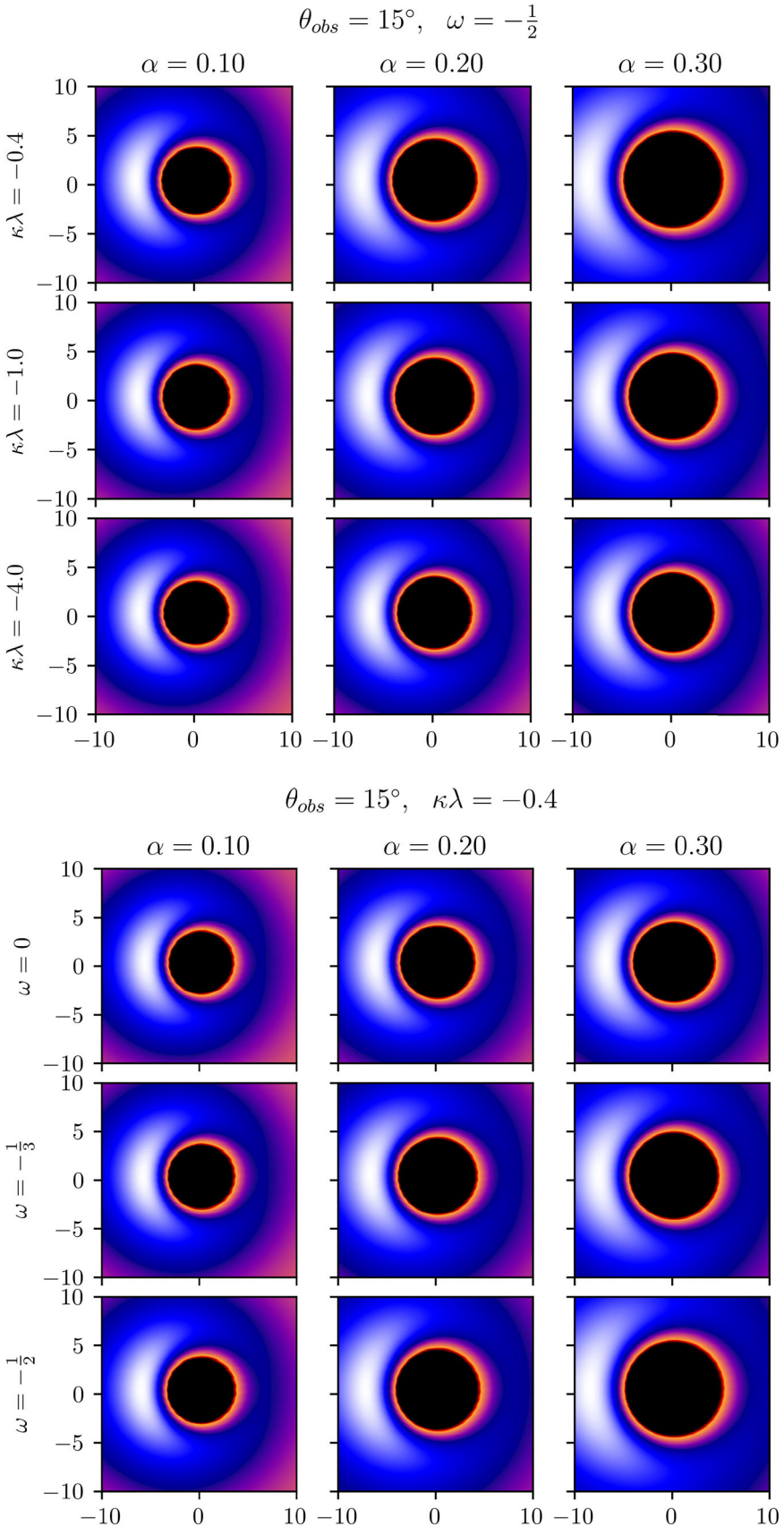

Fig. 10 The same as Fig. 8 but for $\theta = 15°$

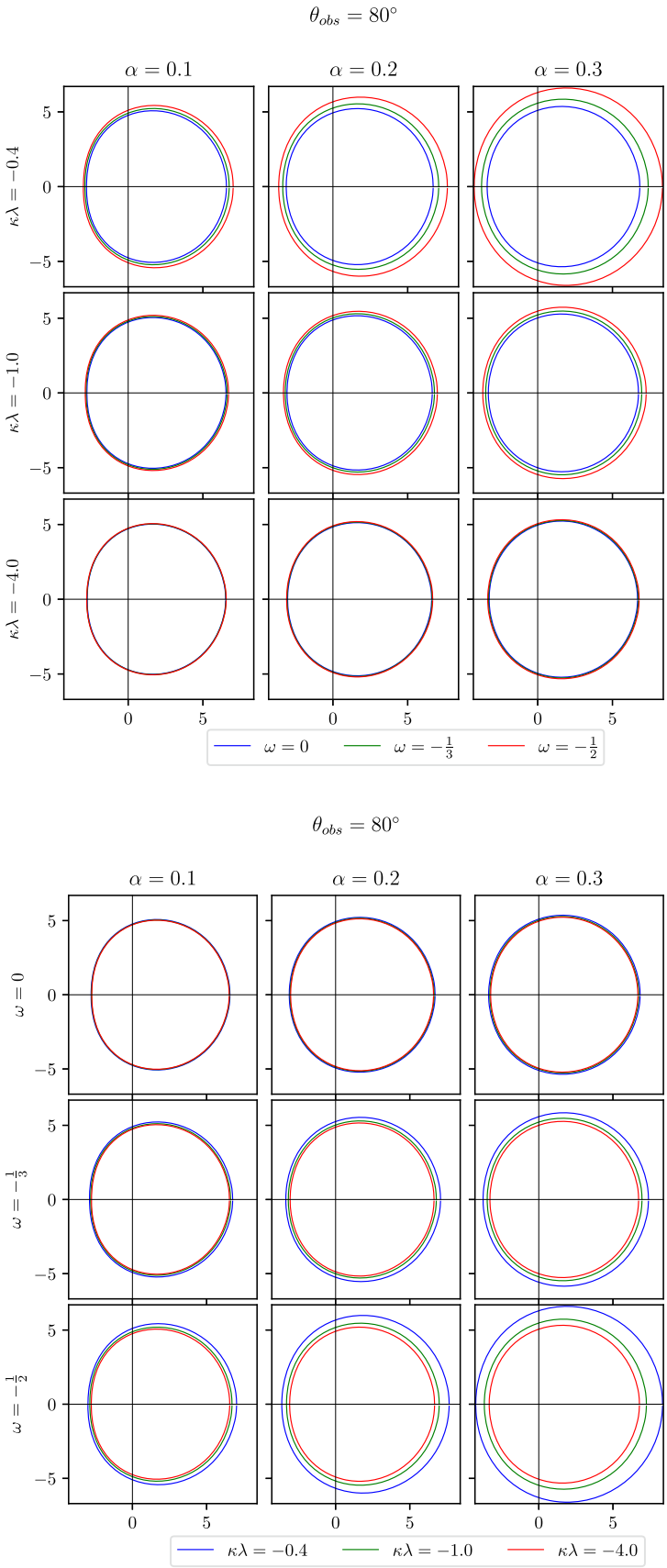

Fig. 11 Appearance of the shadow with the change of the spacetime parameters of the KNNK black hole in the RG when $a = 0.8$, $q = 0.7, l = 0.3$. The case when $\theta_{\text{obs}} = 80°$

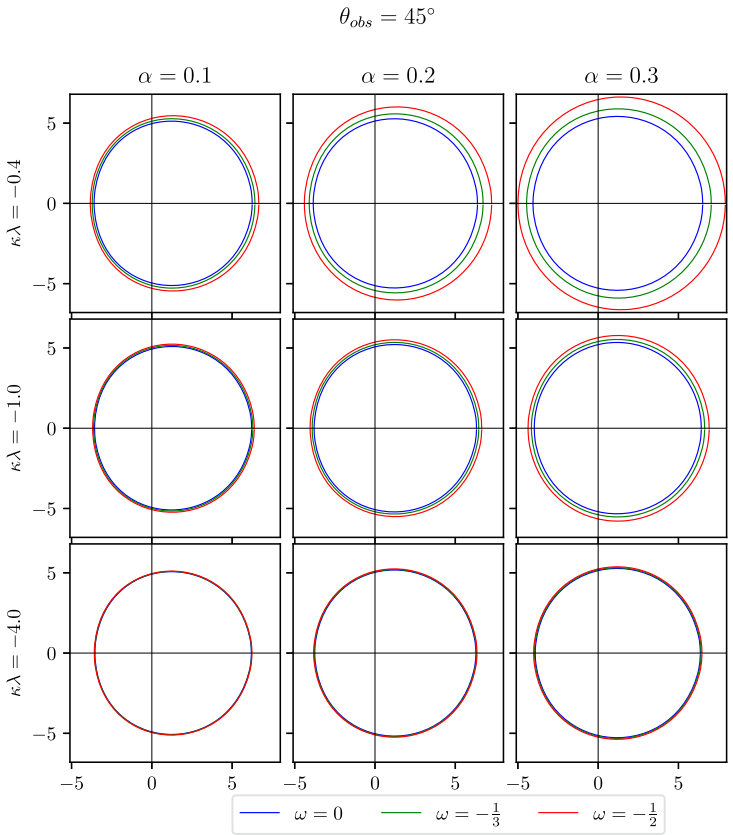

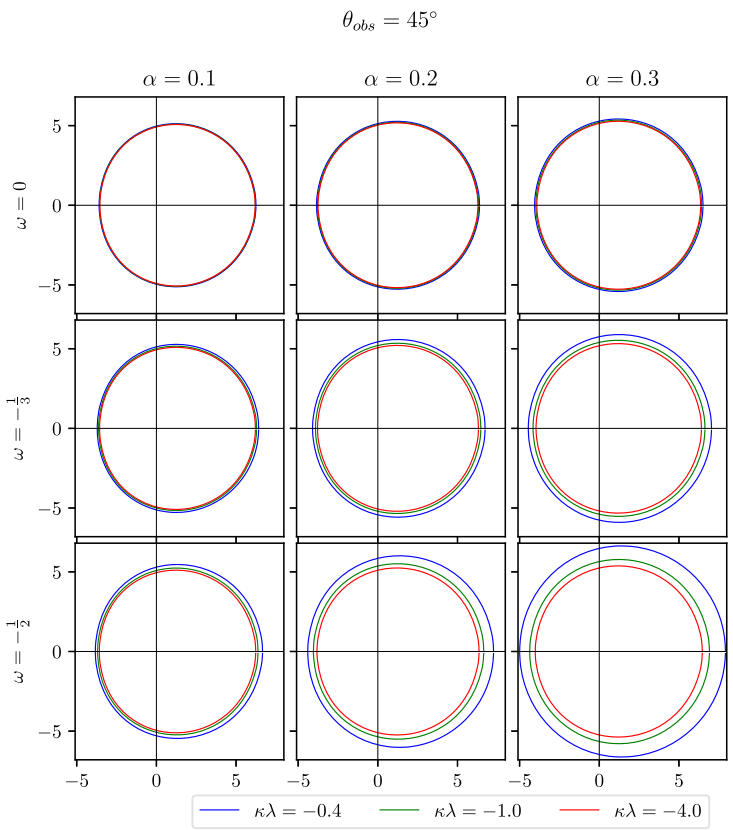

Fig. 12 The same as Fig. 11 but for $\theta_{\rm obs} = 45°$

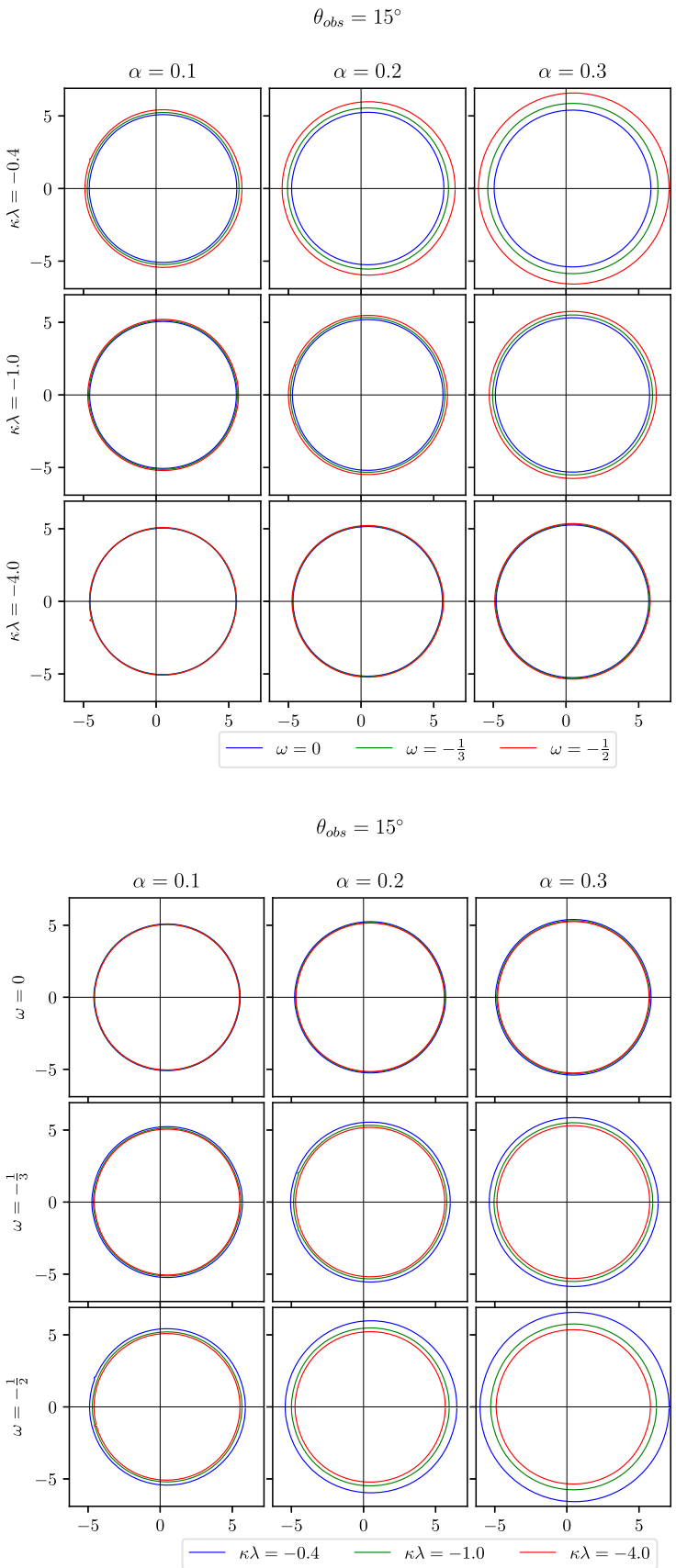

Fig. 13 The same as Fig. 11 but for $\theta_{\text{obs}} = 15°$

the Rastall parameter $\kappa\lambda$ tends to 0. We have noticed that the change in the thermal flux with the parameter $\kappa\lambda$ is more prominent when the parameter ω_q has values considerably below 0. Since we assume that the radiation coming from the accretion disk to be the same as the radiation of the absolute black body, therefore, the temperature profile of the accretion disk can be defined as $F(r) = \sigma T^4$, and consequently, the similar behavior of the temperature profile can be predicted.

Next, we have used two separate codes, namely, the GYOTO code and the TM code to explore the shadow formed around the central KNNK black hole in the RG with a thin accretion disk. It is worth mentioning that the TM code was developed by the first author (TM) of this project, using C++ and Python languages and named after him as the TM code. We have found that both the codes give similar behavior of the shadow with the change of spacetime parameters of the KNNK black hole solution in the RG, except the fact that in the GYOTO code the light rays that come from the bottom part of the central black hole are not taken into account, while this issue has been resolved in the TM code. We have shown that the left hand side of the apparent black hole environment with respect to the central black hole is much brighter than the right hand side which is because of the fact that the frequency of photons approaching the observer (and thus the observed flux energy) is always higher than that of the receding ones (also known as the Doppler beaming effect). We have demonstrated that the increase of the quintessential intensity increases the size of the shadow around the central black hole considerably for very small values of the parameter $\kappa\lambda$. We have also demonstrated that the change in the size of the shadow cast by the KNNK black hole in the RG becomes negligible with the change of α when the parameter ω_q tends to zero and this change in size becomes considerable when ω_q is considerably below zero. We have shown that the position and shape of shadow of the KNNK black hole in the RG strongly depends on the inclination angle of the observer. An other observation is that when the inclination angle is small the geometrical center of the shadow of the black hole shifts to the right for the selected values of spacetime parameters of KNNK black hole in the RG and the shadow has more circle-like form. We have seen that the shadow of the black hole shifts towards the right side and becomes more deformed with the increase in the inclination angle.

Acknowledgements This research is supported by Grants F-FA-2021-432, F-FA-2021-510 and MRB-2021-527 of the Uzbekistan Ministry for Innovative Development. A.A. and B.A. acknowledge the support of Uzbekistan Ministry for Innovative Development Grants and the Abdus Salam International Centre for Theoretical Physics under the Grant No. OEA-NT-01.

Data Availability Statement This manuscript has no associated data, or the data will not be deposited. (There are no observational data related to this article. The necessary calculations and graphic discussion can be made available on request).

References

1. H. Falcke, F. Melia, E. Agol, Astrophys. J. **528**, L13 (2000). https://doi.org/10.1086/312423
2. K. Akiyama et al., Astrophys. J. Lett. (2019). https://doi.org/10.3847/2041-8213/ab0f43
3. W.M. Farr, N. Sravan, A. Cantrell, L. Kreidberg, C.D. Bailyn, I. Mandel, V. Kalogera, Astrophys. J. **741**, 103 (2011). https://doi.org/10.1088/0004-637X/741/2/103. arXiv:1011.1459 [astro-ph.GA]
4. R. Takahashi, J. Korean Phys. Soc. **45**, S1808 (2004). https://doi.org/10.1086/422403. arXiv:astro-ph/0405099
5. M.A. Abramowicz, P.C. Fragile, Living Rev. Rel. **16**, 1 (2013). https://doi.org/10.12942/lrr-2013-1. arXiv:1104.5499 [astro-ph.HE]
6. N.I. Shakura, R.A. Sunyaev, Astron. Astrophys. **24**, 337 (1973)
7. D.N. Page, K.S. Thorne, Astrophys. J. **191**, 499 (1974). https://doi.org/10.1086/152990
8. M. Milosavljević, V. Bromm, S.M. Couch, S.P. Oh, Astrophys. J. **698**, 766 (2009). https://doi.org/10.1088/0004-637x/698/1/766
9. M. Jamil, I. Hussain, Int. J. Theor. Phys. **50**, 465 (2011). https://doi.org/10.1007/s10773-010-0553-5. arXiv:1101.1583 [astro-ph.CO]
10. A. Jawad, M.U. Shahzad, Eur. Phys. J. C **76**, 123 (2016). https://doi.org/10.1140/epjc/s10052-016-3967-2. arXiv:1602.05952 [gr-qc]
11. A. Jawad, K. Jusufi, M.U. Shahzad, Phys. Rev. D **104**, 084045 (2021). https://doi.org/10.1103/PhysRevD.104.084045
12. I.D. Novikov, K.S. Thorne, in *Les Houches Summer School of Theoretical Physics: Black Holes* pp. 343–550 (1973)
13. C.S.J. Pun, Z. Kovács, T. Harko, Phys. Rev. D **78**, 024043 (2008). https://doi.org/10.1103/PhysRevD.78.024043
14. D. Perez, G.E. Romero, S.E.P. Bergliaffa, Astron. Astrophys. **551**, A4 (2013). https://doi.org/10.1051/0004-6361/201220378. arXiv:1212.2640 [astro-ph.CO]
15. A.J. John, Mon. Not. R. Astron. Soc. **490**, 3824 (2019). https://doi.org/10.1093/mnras/stz2889. arXiv:1603.09425 [gr-qc]
16. A. Ditta, G. Abbas, Chin. J. Phys. **65**, 325 (2020). https://doi.org/10.1016/j.cjph.2020.03.007
17. A.M. Bauer, A. Cárdenas-Avenda, C.F. Gammie, N. Yunes (2022) Astrophys. J. **925**, 119. https://doi.org/10.3847/1538-4357/ac3a03. arXiv:2111.02178 [gr-qc]
18. C. Liu, S. Yang, Q. Wu, T. Zhu, J. Cosmol. Astropart. Phys. **2022**, 034 (2022). https://doi.org/10.1088/1475-7516/2022/02/034
19. Z. Kovacs, K.S. Cheng, T. Harko, Astron. Astrophys. **500**, 621 (2009). https://doi.org/10.1051/0004-6361/200811412. arXiv:0903.4746 [astro-ph.HE]
20. T. Harko, Z. Kovacs, F.S.N. Lobo, Phys. Rev. D **79**, 064001 (2009). https://doi.org/10.1103/PhysRevD.79.064001. arXiv:0901.3926 [gr-qc]
21. K.V. Staykov, D.D. Doneva, S.S. Yazadjiev, JCAP **08**, 061 (2016). https://doi.org/10.1088/1475-7516/2016/08/061. arXiv:1606.01529 [gr-qc]
22. S. Paul, R. Shaikh, P. Banerjee, T. Sarkar, JCAP **03**, 055 (2020). https://doi.org/10.1088/1475-7516/2020/03/055. arXiv:1911.05525 [gr-qc]
23. J.F. Hawley, L.L. Smarr, J.R. Wilson, (1983)
24. D. Molteni, D. Ryu, S.K. Chakrabarti, Astrophys. J. **470**, 460 (1996). https://doi.org/10.1086/177877. arXiv:astro-ph/9605116
25. P. Amaro-Seoane, M. Freitag, R. Spurzem, Mon. Not. R. Astron. Soc. **352**, 655 (2004). https://doi.org/10.1111/j.1365-2966.2004.07956.x. arXiv:astro-ph/0401163
26. P.C. Fragile, P. Anninos, Astrophys. J. **623**, 347 (2005). https://doi.org/10.1086/428433
27. S. Koide, D.L. Meier, K. Shibata, T. Kudoh, Astrophys. J. **536**, 668 (2000). https://doi.org/10.1086/308986. arXiv:astro-ph/9907435
28. F.H. Vincent, T. Paumard, E. Gourgoulhon, G. Perrin, Class. Quant. Grav. **28**, 225011 (2011). https://doi.org/10.1088/0264-9381/28/22/225011. arXiv:1109.4769 [gr-qc]
29. D. Psaltis, T. Johannsen, Astrophys. J. **745**, 1 (2012). https://doi.org/10.1088/0004-637X/745/1/1. arXiv:1011.4078 [astro-ph.HE]

30. D. Ayzenberg, N. Yunes, Classical Quantum Gravity **35**, 235002 (2018). https://doi.org/10.1088/1361-6382/aae87b. arXiv:1807.08422 [gr-qc]
31. A.B. Abdikamalov, A.A. Abdujabbarov, D. Ayzenberg, D. Malafarina, C. Bambi, B. Ahmedov, Phys. Rev. D **100**, 024014 (2019). https://doi.org/10.1103/PhysRevD.100.024014. arXiv:1904.06207 [gr-qc]
32. B.S. Haridasu, V.V. Lukovi ́c, R. D'Agostino, N. Vittorio, Astron. Astrophys. **600**, L1 (2017). https://doi.org/10.1051/0004-6361/201730469. arXiv:1702.08244 [astro-ph.CO]
33. V.V. Kiselev, Class. Quant. Grav. **20**, 1187 (2003). https://doi.org/10.1088/0264-9381/20/6/310. arXiv:gr-qc/0210040
34. B. Toshmatov, Z. Stuchlík, B. Ahmedov, Mod. Phys. Lett. A **32**, 1775001 (2017). https://doi.org/10.1142/S0217732317750013. arXiv:1707.00403 [gr-qc]
35. M.F.A.R. Sakti, A. Suroso, F.P. Zen, Eur. Phys. J. Plus **134**, 580 (2019). https://doi.org/10.1140/epjp/i2019-12937-x. arXiv:1909.06595 [hep-th]
36. N.U. Mollaand, U. Debnath, Int. J. Modern Phys. A **36**, 2150210–168 (2021). https://doi.org/10.1142/S0217751X21502109
37. M.F.A.R. Sakti, A. Suroso, F.P. Zen, Ann. Phys. **413**, 168062 (2020). https://doi.org/10.1016/j.aop.2019.168062. arXiv:1901.09163 [gr-qc]
38. P. Rastall, Phys. Rev. D **6**, 3357 (1972). https://doi.org/10.1103/PhysRevD.6.3357
39. M. Visser, Phys. Lett. B **782**, 83 (2018). https://doi.org/10.1016/j.physletb.2018.05.028. arXiv:1711.11500 [gr-qc]
40. F. Darabi, H. Moradpour, I. Licata, Y. Heydarzade, C. Corda, Eur. Phys. J. C **78**, 25 (2018). https://doi.org/10.1140/epjc/s10052-017-5502-5. arXiv:1712.09307 [gr-qc]
41. Y. Heydarzade, H. Moradpour, F. Darabi, Can. J. Phys. **95**, 1253 (2017). https://doi.org/10.1139/cjp-2017-0254. arXiv:1610.03881 [gr-qc]
42. R. Kumarand, S.G. Ghosh, Eur. Phys. J. C **78**, 750 (2018). https://doi.org/10.1140/epjc/s10052-018-6206-1
43. B. Narzilloev, I. Hussain, A. Abdujabbarov, B. Ahmedov, C. Bambi, Eur. Phys. J. Plus **136**, 1032 (2021). https://doi.org/10.1140/epjp/s13360-021-02039-x. arXiv:2110.01772 [gr-qc]
44. B. Narzilloev, D. Malafarina, A. Abdujabbarov, C. Bambi, Eur. Phys. J. C **80**, 784 (2020). https://doi.org/10.1140/epjc/s10052-020-8370-3arXiv:2003.11828 [gr-qc]
45. B. Narzilloev, J. Rayimbaev, A. Abdujabbarov, C. Bambi, Eur. Phys. J. C **80**, 1074 (2020). https://doi.org/10.1140/epjc/s10052-020-08623-2. arXiv:2005.04752 [gr-qc]
46. S. Shaymatov, B. Narzilloev, A. Abdujabbarov, C. Bambi, Phys. Rev. D **103**, 124066 (2021). https://doi.org/10.1103/PhysRevD.103.124066
47. B. Narzilloev, D. Malafarina, A. Abdujabbarov, B. Ahmedov, C. Bambi, Phys. Rev. D **104**, 064016 (2021). https://doi.org/10.1103/PhysRevD.104.064016
48. J. Rayimbaev, B. Narzilloev, A. Abdujabbarov, B. Ahmedov, Galaxies (2021). https://doi.org/10.3390/galaxies9040071
49. B. Narzilloev, J. Rayimbaev, A. Abdujabbarov, B. Ahmedov, Galaxies (2021). https://doi.org/10.3390/galaxies9030063
50. B. Narzilloev, S. Shaymatov, I. Hussain, A. Abdujabbarov, B. Ahmedov, C. Bambi, Eur. Phys. J. C **81**, 849 (2021). https://doi.org/10.1140/epjc/s10052-021-09617-4. arXiv:2109.02816 [gr-qc]
51. Z. Xu, Y. Liao, J. Wang, Int. J. Mod. Phys. A **34**, 1950185 (2019). https://doi.org/10.1142/S0217751X19501859
52. I. Banerjee, S. Chakraborty, S. SenGupta, Phys. Rev. D **100**, 044045 (2019). https://doi.org/10.1103/PhysRevD.100.044045. arXiv:1905.08043 [gr-qc]
53. S.X. Tianand, Z.H. Zhu, Phys. Rev. D **100**, 064011 (2019). https://doi.org/10.1103/PhysRevD.100.064011
54. C. Bambi, *Black Holes: A Laboratory for Testing Strong Gravity* (Springer, Singapore, 2017)
55. K. Akiyama et al., Astrophys. J. **875**, L1 (2019). https://doi.org/10.3847/2041-8213/ab0ec7. arXiv:1906.11238 [astro-ph.GA]
56. K. Akiyama et al., Astrophys. J. Lett. **875**, L2 (2019). https://doi.org/10.3847/2041-8213/ab0c96. arXiv:1906.11239 [astro-ph.IM]